

---

# Ultrasonic Viscoelasticity Imaging of Nonpalpable Breast Tumors: Preliminary Results<sup>1</sup>

Yupeng Qiu, BSc, Mallika Sridhar, PhD, Jean K. Tsou, PhD, Karen K. Lindfors, MD, Michael F. Insana, PhD

---

**Rationale and Objectives.** Improvements in the diagnosis of early breast cancers depend on a physician's ability to obtain the information necessary to distinguish nonpalpable malignant and benign tumors. Viscoelastic features that describe mechanical properties of tissues may help to distinguish these types of lesions.

**Materials and Methods.** Twenty-one patients with nonpalpable, pathology-confirmed Breast Imaging Reporting and Data System (BIRADS) 4 or 5 breast lesions (10 benign, 11 malignant) detected by mammography were studied. Viscoelastic parameters were extracted from a time sequence of ultrasonic strain images, and differences in the parameters between malignant and benign tumors were compared. Parametric data were color coded and superimposed on sonograms.

**Results.** The strain retardance time parameter,  $T_1$ , provided the best discrimination between malignant and benign tumors ( $P < .01$ ).  $T_1$  measures the time required for tissues to fully deform (strain) once compressed; therefore, it describes the time-varying viscous response of tissue to a small deforming force. Compared to the surrounding background tissues, malignant lesions have smaller average  $T_1$  values, whereas benign lesions have higher  $T_1$  values. This tissue-specific contrast correlates with known changes in the extracellular matrix of breast stroma.

**Conclusion.** Characterization of nonpalpable breast lesions is improved by the addition of viscoelastic strain imaging parameters. The differentiation of malignant and benign BI-RADS 4 or 5 tumors is especially evident with the use of the retardation time estimates,  $T_1$ .

**Key Words.** Breast cancer; elasticity; diagnosis.

© AUR, 2008

---

Breast cancer is the fifth most common cause of cancer death worldwide, and the most frequently diagnosed cancer in women (1). In the United States during 2007, it was expected that approximately 178,480 women

would develop invasive breast cancer and an estimated 40,910 patients would die from this disease. The combined efforts of early detection and improved treatment have steadily decreased the death rate in women from breast cancer since 1990. The earliest cancer signs are detectable by medical imaging often before symptoms appear. Diagnosis is currently based on information obtained from the clinical examination, anatomic imaging, and biopsy. Although histopathology is the gold standard for diagnosis, the biopsy procedure is invasive, expensive, and carries some risk. Therefore, additional noninvasive diagnostic imaging methods to increase specificity and reduce the need for biopsy would be beneficial.

Recent discoveries in molecular biology have triggered interest in developing new and potentially more specific

---

**Acad Radiol 2008; 15:1526–1533**

<sup>1</sup> From the Department of Bioengineering and Beckman Institute for Advanced Science and Technology, University of Illinois at Urbana-Champaign, 405 North Mathews, Room 5237, Urbana, IL 61801 (Y.Q., M.F.I.); and Departments of Biomedical Engineering (M.S., J.K.T.) and Radiology (K.K.L.), University of California, Davis, CA. Received April 14, 2008; accepted May 24, 2008. This work was supported by the NCI under award No. CA082497 and by the Beckman Institute for Advanced Science and Technology at the University of Illinois. **Address correspondence to:** Y.Q. e-mail: [yqiu2@illinois.edu](mailto:yqiu2@illinois.edu)

© AUR, 2008

doi:10.1016/j.acra.2008.05.023

imaging methods for breast cancer diagnosis (2). These include techniques for: 1) direct imaging of signaling molecules and/or receptors mediating malignant progression, and 2) indirect imaging of intrinsic tissue properties (eg, biochemical, mechanical) that describe the tumor microenvironment controlling signaling pathways. We use the latter method to detect local changes in soft tissue. The alteration in elasticity properties is in part a result of inflammation that usually occurs during the early stages of disease development. The extracellular matrix (ECM) of breast stroma, which provides the solid consistency of parenchymal tissues, plays an active role in cancerous tumor growth (3). Hence, breast stroma is a potentially valuable source of endogenous disease-specific contrast.

The term “elasticity imaging” refers to any application of imaging technologies to the spatiotemporal description of the mechanical properties of a medium (4). Medical elasticity imaging is broadly categorized as dynamic or quasi-static, where in both cases a small applied force creates tissue deformations that may be tracked by ultrasonic, magnetic resonance, or optical imaging technologies. Dynamic methods for imaging viscoelastic breast features stimulate tissues with harmonic (5,6) or impulse (7,8) forces, typically in the micro-to-milliNewton ( $\mu\text{N}$ – $\text{mN}$ ) amplitude range and at frequencies above 50 Hz.

We employ quasi-static ultrasonic methods for viscoelastic breast imaging. Echo movements are tracked as an ultrasonic probe is gently pressed into the skin surface. Step-force amplitudes of 3–6 N\* are applied suddenly and handheld constant for 10–20 seconds while ultrasonic echo data are acquired to track movements in a series of strain images. Such methods are quasi-static because the frequency range for this force stimulus is less than about 1 Hz (9). The slow movement of tissue under a load—called viscous creep—is characteristic of the viscoelastic (VE) properties of tissues. VE properties are found by analyzing a time series of elastic strain images. Because creep responses to mechanical forces vary in soft tissues and other hydrolypolymers with the frequency of the force stimulus, dynamic and quasi-static methods are believed to provide independent information. It is not yet known which part of the force bandwidth has the most diagnostic information.

Recent studies (10–13) have suggested that elastic strain images of breast tissue can be effective at discriminating focal benign and malignant tumors. Thomas et al.

(11) showed that strain and strain-rate images were most effective when diagnosing Breast Imaging Reporting and Data System (BIRADS) 3 lesions with lipomatous involution and somewhat less effective with BIRADS 4 or 5 lesions. A sensitive diagnostic feature was the ratio of lesion size visualized in strain images versus that in spatially registered sonograms, suggesting that many of the malignancies studied had a palpable degree of desmoplasia, thereby appearing larger on strain images than sonograms. Zhi et al (12) also showed that strain imaging was effective at malignant–benign discrimination for late-stage tumors. However, with strain images, early stage (I and II) infiltrating ductal carcinomas (IDCs) were misdiagnosed presumably because of the lack of desmoplasia. Although lesion palpability and size were not selection criteria for patients in these prior studies, more than half of the lesions were identified as palpable, and the maximum tumor diameter ranged from 0.3 to 10 cm. The purpose of our study was to determine whether viscoelastic features improved benign versus malignant differentiation for nonpalpable breast lesions discovered on mammographic scanners.

## MATERIALS AND METHODS

### Patient Selection

Data were collected from 26 adult female patients through the breast clinic at UC Davis (UCD) Medical Center (Sacramento, CA). Consent to participate was obtained from patients with a single, nonpalpable lesion identified by mammography just prior to undergoing a core needle biopsy procedure. The protocol was approved by institutional reviews boards at both UCD and University of Illinois at Urbana-Champaign (UIUC). Data from five patients were rejected due to bad acquisition techniques that did not allow for further extractions of viscoelastic parameters needed for this study. Data from 21 patients were used for this clinical study. Of these 21 patients, 10 patients were diagnosed with benign lesions and 11 patients with malignant lesions of various types. Patient ages ranged between 28 and 72 years, and tumor sizes ranged between 0.5 and 2.5 cm. The patients were selected randomly under the criteria that they have nonpalpable lesions that were identified via mammography. All lesions were BI-RADS 4 or 5, which identified these lesions as potentially malignant and requiring tissue diagnosis.

Biopsy samples from patients with malignant tumors were assigned Scarff-Bloom-Richardson (SBR) scores based on three morphologic features: degree of tumor

\* For comparison, mammographic compressional forces are 100–200 N.

tubule formation, tumor mitotic activity, and nuclear pleomorphism of tumor cells. SBR scale assigns 1–3 points for each feature; the final score is the sum of all 3 (minimum 3, maximum 9), where higher scores indicate greater likelihood of tumor growth and metastasis. Tumors scoring between 3 and 5 are labeled Grade 1 (normal cell appearance); those with a score of 8 or 9 are labeled Grade 3 (poorly differentiated with tendency to grow and spread aggressively); and those with a score of 6 or 7 are in between. The SBR score and tumor grade aid physicians with treatment strategies and prognosis. Among the 11 patients with confirmed malignant tumors in our study, four were diagnosed as Grade 1 tumors, four as Grade 2, one as Grade 3, and 2 were not scored. Small size, low level of lymphatic invasion, low number of tumors per patient, lack of metastasis, and the tumor grades classify our patient group as having early stage malignancies.

### Lesion Diagnoses

Benign and malignant lesions were further classified into four subtypes or combinations with the exceptions of one benign lesion diagnosed as dense collagenous stroma and one malignant lesion diagnosed as B-cell lymphoma.

**IDC.**—IDC is the most common form of breast cancer, accounting for 65% to 80% of malignant mammary carcinomas (14). Eight of 11 patients with malignant tumors were diagnosed with either IDC or IDC combined with ductal carcinoma in-situ (DCIS). All were Grade 1 or 2 and categorized as BI-RADS 4 or 5. Although many IDC tumors have a stiff desmoplastic stroma surrounding the tumor, IDC tumors in our population were nonpalpable.

**ILC.**—Invasive lobular carcinoma (ILC) accounts for about 10% to 15% of all breast cancers (14). Two of the 11 patients with malignant tumors were diagnosed with ILC. One had a Grade 1 tumor and both were classified BI-RADS 5. Both ILC patients were in their mid 50s to early 60s. Both had only one breast involved and no signs of metastasis. Early-stage ILC lesions are usually nonpalpable due to lack of desmoplasia reaction, difficult to observe mammographically, and thus, are often larger in size at diagnosis.

**Fibroadenoma.**—Seven of 10 patients with benign tumors were diagnosed with fibroadenoma. All of these patient images were categorized as BI-RADS 4.

**Fibrocystic change.**—Two of 10 patients with benign tumors were diagnosed with fibrocystic changes. Both were BI-RADS 4 lesions. The condition is characterized by stiff noncancerous regions containing a high-density of

normal ECM collagen and increased interstitial fluid pressure. However, our patient group presented no palpable lesions at physical examination.

All four lesion types usually express increased levels of ECM proteins, which tend to stiffen the lesion to varying degrees relative to their surround medium. IDC lesions with desmoplasia are particularly stiff, often palpable, and frequently appear larger in the elastic strain image than on the sonogram (15). By limiting our test population for VE imaging parameters to nonpalpable lesions, our study focuses on early disease that can be difficult to diagnose.

### Imaging Techniques

Techniques for imaging VE features of breast tissues have been previously described (9,16). A Siemens Sonoline Antares ultrasound scanner (Siemens Medical Solutions, Mountain View, CA) was used with a VF10-5 linear array transducer operated at 8 MHz. The scanner was configured with an Ultrasound Research Interface (URI) capable of recording radiofrequency (RF) echo data corresponding to the image displayed on the monitor for off-line processing. Patients were positioned supine and the breasts were scanned anterior–posterior with the chest wall as compression support. Patients were instructed to hold their breath during the 12- to 15-second data acquisition time to minimize breast motion. The RF acquisition frame rate was 17 frames/s. Scanning was repeated at least three times for each patient to ensure consistency in the compressive motion of the breasts.

A small compressive force was applied manually to the breast surface by operators holding the transducer probe without restraint, the same as in clinical imaging. The operators apply a constant downward (compressive) force of approximately 4 N for the duration of the scan. Sridhar and Insana (9) showed that sonographers with limited training were able to keep the force constant within  $\pm 0.24$  N. The recording of RF echo frames began just prior to compression. The entire force was applied within 1 second and held constant while RF frames were recorded for 12 to 15 seconds. Echoes were recorded at an average depth of 30 mm.

### Curve Fitting

From the time series of RF frames recorded during the application of the force, strain images were formed using multicompression techniques (17) and a regularized optical flow algorithm (18). Figure 1 illustrates how we analyzed the RF echo frames (totaling  $K$  frames) recorded

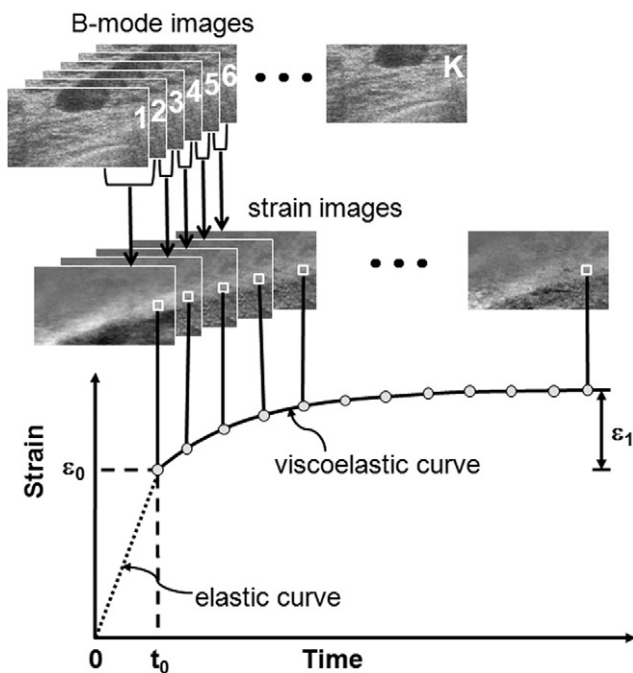


**Figure 1.** Multicompression radiofrequency echo acquisition, strain image formation, and viscoelastic parameter estimation for a patient with a nonpalpable fibroadenoma.  $\epsilon_0$  describes the instantaneous elastic strain.  $\epsilon_1$  describes the viscoelastic strain amplitude. Compression is applied from time  $t = 0$  until  $t_0$ , during which the instantaneous elastic strain is measured.  $t_0$  is also the time at which computation of the viscoelastic response begins. The viscoelastic curve lasts 12 to 15 seconds. K, total number of acquired radiofrequency during the application of the compression force.

over time by applying a sliding reference frame to form a time series of  $K-1$  strain images. The  $k$ th strain image in the series is made from adjacent RF echo frame pairs,  $f_k$  and  $f_{k+1}$  where  $k = 1, 2, 3, \dots, K-1$ . Each strain image is spatially registered to match the geometry of the pre-compression sonogram. Strain is plotted over the time series of images to generate the viscous creep curve as shown in Figure 1. The VE phase of the curve begins immediately after tissue compression at time  $t_0$ . One curve is computed for each strain pixel, or small group of pixels, from which VE parameters are estimated as described in the following.

VE parameters were extracted from each measured creep curve by least-square fitting of the patient data to a rheologic model (19). Our clinical imaging acquisitions are no longer than 15 seconds. Consequently, the long-duration VE response terms are not engaged; therefore, a first-order discrete Kelvin-Voigt rheologic model (9,19) is appropriate:

**Viscoelastic Strain Curves**

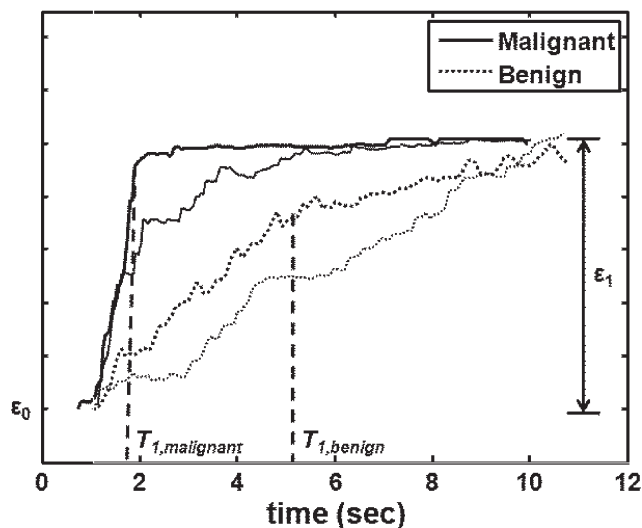


**Figure 2.** Examples of malignant and benign viscoelastic strain curves.  $\epsilon_0$  describes the instantaneous elastic strain.  $\epsilon_1$  describes the viscoelastic strain amplitude. The retardance time constant  $T_1$  measures the time required for the viscoelastic curve to reach a plateau.  $T_1$  value for the malignant tumor is shorter than that for the benign tumor.

$$\epsilon(t) = \epsilon_0 + \epsilon_1(1 - \exp(-t/T_1)). \tag{1}$$

The term  $\epsilon_0$  is the instantaneous elastic strain that occurs immediately after compression (Fig 1). In the second term,  $\epsilon_1$  is the amplitude of the exponential creep curve. The constant  $T_1$  is the retardation time of the curve characterizing the delay in the full strain response. Strain delays in the stroma are from frictional resistance due to movement of the ECM in viscous interstitial fluids (9). Elastic strain  $\epsilon_0$ , viscoelastic strain amplitude  $\epsilon_1$ , and the strain retardance time constant  $T_1$  are the VE features analyzed in our study. Examples of malignant and benign VE curves are shown in Figure 2.

**Pixel Selection and Averaging**

Small areas of  $10 \times 30$  pixels were selected by hand within the lesion and background regions of each patient image (Fig 3). In those regions, the average B-mode,  $\epsilon_0$ ,  $\epsilon_1$ , and  $T_1$  values from the spatially registered images are estimated. In cases of tissue heterogeneity, the selection area was reduced to  $10 \times 15$  pixels, but consistency of the mean parameter values was maintained by repeating the process for difference area selections. For each image set, there are at least five selections per image that yield values that are within 15%–20% of each other. These selections are averaged to give the mean values reported.

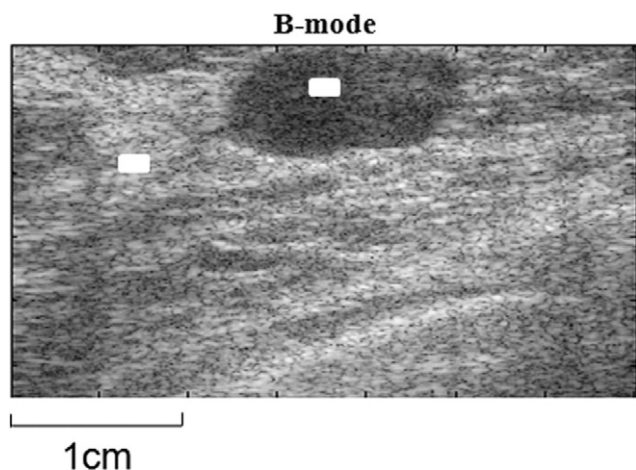


**Figure 3.** Example of pixel selection for statistical analysis. The selection boxes (marked in white) vary in size from 10 × 30 to 10 × 15 pixels.

**Parametric Contrast**

Contrast is an important visual feature for diagnosis, more than the parameters values. The goal of VE imaging is to provide tissue-specific parametric contrast for diagnosis. Contrast is calculated using

$$C = \frac{X_{lesion} - X_{background}}{(X_{lesion} + X_{background})/2} = \frac{Difference}{Average}, \quad (2)$$

where  $X_{lesion}$  and  $X_{background}$  represents any of the four previously described parameters from the lesion and background tissue areas of a patient scan.

**RESULTS**

**Statistical Analysis**

Average VE parameter values for the 21 patient studies are displayed in Figure 4 as histograms with error bars indicating standard errors. Due to the low number of patient studies in each lesion subtype, data were grouped into malignant and benign classes only. Two-sided *t*-tests were performed for each of the four parameters to test the hypothesis that data from the malignant and benign groups are really just one population. Parameters for which *P* values were < .05 were considered able to distinguish between the two lesion groups. The *t*-tests results from data summarized in Figure 4 are shown in Table 1.

Only the VE retardance time constant,  $T_1$ , was found to be separable and at the 99% significance level ( $P < 0.01$ ). The histogram of Figure 4b shows the difference of

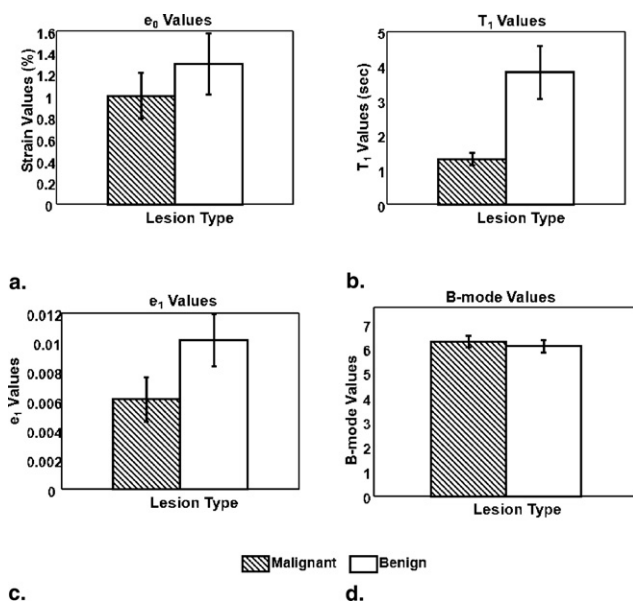


**Figure 4.** Average lesion parameters. (a) Elastic strain values  $\epsilon_0$  ( $P < .5$ ); (b) Time constants  $T_1$  ( $P < .01$ ); (c) creep-curve amplitudes  $\epsilon_1$  ( $P < .1$ ); and (d) B-mode pixel values ( $P < .6$ ). Error bars denote  $\pm 1$  standard error.

**Table 1**  
**t-Test Results from Viscoelastic Parameters**

Parameter	<i>P</i> Values (95% significance)
$\epsilon_0$	.4213
$T_1$	.0098
$\epsilon_1$	.0986
B-mode	.5830

means for  $T_1$  clearly exceeding the standard errors. For comparisons, we refer to the VE parameters found for normal glandular breast tissue from a previous study,  $T_1 = 3.2 \pm 0.8$  seconds (9). The present study as shown in Figure 4b shows an average  $T_1$  value of  $3.9 \pm 0.7$  seconds for benign tumors and  $1.4 \pm 0.2$  seconds for malignant tumors. Therefore, the difference in average  $T_1$  values between normal parenchyma and malignant lesions is also highly significant. We also looked for correlations between  $T_1$  image contrast, Equation 2, and tumor grade value (1–3), and we found the linear relationship  $C_{T1} = -0.18 \times \text{Grade} - 0.35$ . The norm of the residuals for the equation fit was 0.014, suggesting strong correlation. However, there are too few samples to obtain the statistical power required for significance; therefore, the result should be considered preliminary. Parameter uncertainties reported previously are of the same order of magnitude as those caused by handheld applicators.

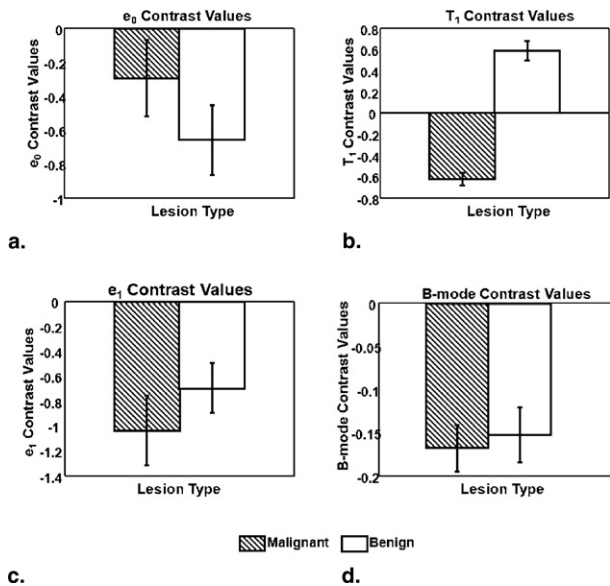


**Figure 5.** Contrast values for (a) elastic strain, (b)  $T_1$ , (c)  $\epsilon_1$  and (d) B-mode images. Error bars denote  $\pm 1$  standard error.

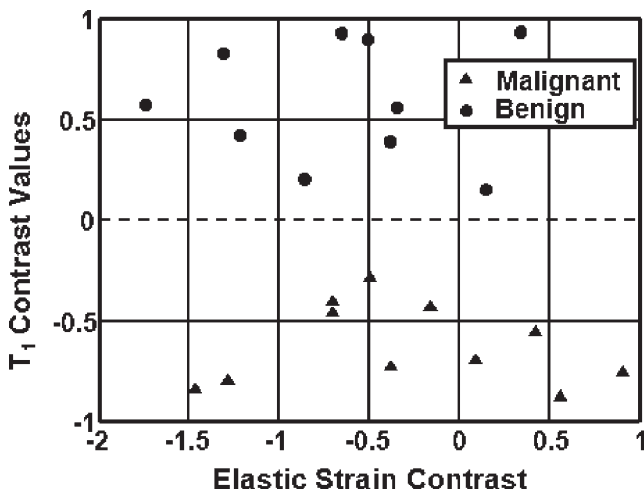


**Figure 6.** Scatterplot of patient contrast values for two parameters,  $\epsilon_0$  and  $T_1$ . A dotted line drawn at  $T_1$  contrast = 0 divides malignant and benign lesions. However,  $\epsilon_0$  contrast offers no significant discriminability.

A previous study on normal volunteers (9) showed that the standard deviation for time constants estimates is typically 25% of the mean. Because the uncertainties are of the same magnitude on patients' measurements, we infer that patient variability is small compared with operator variability.

**Contrast Histograms and Scatterplot**

Although the  $t$ -test for retardation time  $T_1$  revealed a statistically significant difference between the mean val-

ues for benign and malignant tumors, it is important for image-based diagnosis to also explore contrast differences with respect to background areas. Equation 2 was applied to calculate patient contrast for each of the four parameters,  $B$ -mode,  $\epsilon_0$ ,  $\epsilon_1$ ,  $T_1$ ; the results are shown in Figure 5, where we see that only  $T_1$  provided statistically significant contrast.

Figure 6 shows a scatterplot of elastic strain ( $\epsilon_0$ ) contrast versus  $T_1$  contrast for each of the 21 patients. In Figure 6,  $T_1$  contrast is negative for all malignant tumors and positive for benign tumors, thus clearly providing lesion discrimination. None of the other features provided such strong discriminability.

*Color imaging.*—The previous section showed that spatially averaged  $T_1$  contrast allows us to clearly discriminate nonpalpable malignant and benign breast lesions. This section explores spatial variations in the retardance time constant using color mapping of the  $T_1$  contrast as an overlay on the sonogram. The concept is analogous to color-flow imaging where blood velocity is mapped onto the sonographic anatomy.

Consider each image as a matrix of size  $I \times J$ . For each pixel  $p(i, j)$  in the matrix,  $i = 1, \dots, I$  and  $j = 1, \dots, J$ , we compare its  $T_1$  value to the spatially averaged  $T_1$  value near the periphery of the image,  $\bar{T}_1$  (selection box size  $10 \times 30$  or  $10 \times 15$  pixels). For pixels where  $T_1(i, j) < \bar{T}_1$ , we assign an overlay color in the blue spectrum where the shade indicates the negative difference value  $T_1(i, j) - \bar{T}_1$ . For pixels where  $T_1(i, j) > \bar{T}_1$ , we assign an overlay color in the red spectrum where the shade indicates the positive difference value  $T_1(i, j) - \bar{T}_1$ . For example, see the color bars in Figure 7 where an an isoechoic IDC lesion and a hypoechoic fibroadenoma are shown. These color pixels were spatially smoothed and amplitude thresholded in a manner similar to color-flow imaging.

**DISCUSSION**

This preliminary clinical study tentatively confirms the hypothesis that VE parameters from patients with nonpalpable breast lesions can be used to differentiate between malignant and benign breast tumors. A statistical test performed on four parameters,  $\epsilon_0$ ,  $\epsilon_1$ ,  $T_1$ , and  $B$ -mode, showed a significant difference between the retardation time constants  $T_1$  for the two lesion types. In addition,  $T_1$  contrast was found to be negative for malignant lesions and positive for benign lesions in all 21 patient studies.

**Figure 7.** Sonograms with  $T_1$  parametric color overlays. The example in (a) is from a patient with a malignant infiltrating ductal carcinoma (IDC) lesion; the negative  $T_1$  contrast values are shown in *blue*. The example in (b) is from a patient with a benign (fibroadenoma) lesion; the positive  $T_1$  contrast values are shown in *red*.

The observed contrast differences are consistent with known changes in the collagenous stromal ECM near the lesion (20). Benign tumors have increased normal collagen density; that is, the associated proteoglycan content increases in proportion. Dense ECM increases both the cross linking among collagen fibers and the viscosity of interstitial fluids, which increase the resistance to creep and lengthen  $T_1$  values. Very similar results were found in VE phantom studies where hydropolymer density was locally increased (19). Malignant tumors also have increased collagen density; however, these collagen fibers are structurally different from those of normal ECM stroma. Malignant stroma has reduced proteoglycan content for loose and dense connective breast tissues that then reduces the frictional forces resisting creep. Consequently,  $T_1$  values in nonpalpable lesions are less than with that of normal breast stroma. In other words, IDC and ILC lesions are generally more fluidic in their mechanical response than the more solid-responding fibroadenomas. We point out that lesion palpability is determined very subjectively. A study with more patients is required to reach conclusion about clinical efficacy.

As we discovered previously by comparing VE results from breast tissues of normal volunteers (9) and hydropolymer phantoms (19) over much longer acquisition

times (200 and 3600 seconds, respectively), the RF acquisition time significantly influences lesion contrast. Eigenanalysis of normal breast tissues (9) suggests there are at least two VE components in the rheologic model for 200-second breast acquisitions using our quasi-static elasticity imaging method. The VE retardance time constants are  $T_1 = 3.2 \pm 0.8$  seconds and  $T_2 = 42 \pm 28$  seconds. By truncating the acquisition time to practical values <20 seconds, as in the present study, we can ignore the effects of  $T_2$  on  $T_1$ , and we can expect a coefficient of variation for  $T_1$  estimates of 25% due mostly to jitter from the hand-held force application (9). The present study did not examine the  $T_2$  component because 200-second acquisitions were impractical. Also, there is greater relative error for  $T_2$  estimates, which is a tissue response at a much lower force bandwidth (<0.1 Hz) and which requires development of new scanning techniques. Nevertheless, we are encouraged by the diagnostic performance of  $T_1$  estimates for malignant–benign discrimination.

Potential sources of error in viscoelasticity imaging are patient movement (respiratory and cardiac) and hand-held transducer movement during force application. Small transducer movements increase de-correlation errors in strain images (17,18), which then propagate into large noise variations in VE parametric images. Changing to

the high-frequency force stimuli used in dynamic imaging methods (4–7) reduces VE parameter estimation errors for several reasons. However, we know from the polymer mechanics literature that the frequency of the applied force influences the time-varying strain response and therefore VE parameters. To visualize this point, consider movement of the stroma: an ECM polymer embedded within a viscous interstitial fluid. Slow application of a compressive force allows fluid motion with little frictional resistance, and therefore cross linking among ECM fibers determines the VE response. However, dynamic friction increases with the velocity of the applied force, depending on the viscosity of the fluid, until fluid flow dominates the time-varying strain response. Consequently, there is merit in pursuing both quasi-static and dynamic elasticity imaging methods. Both methods are currently limited for clinical applications by our ability to precisely apply forces to the tissue.

Results from this preliminary study have demonstrated that VE imaging of breast tumors can effectively aid in the characterization of nonpalpable breast lesions. The greatest advantage of this novel imaging method is that the VE parameters obtained can be used to clearly differentiate between malignant and benign lesions for patients with nonpalpable, early stage, BI-RADS 4 and 5 breast tumors. The addition of VE features into the diagnosis feature space can aid the physicians in making a more accurate diagnosis of early breast cancer patients.

#### ACKNOWLEDGMENTS

Special thanks to Pamela Phelps and Tonya Sheppard as the sonographers.

Y. Qiu conducted all of the data processing presented in this paper and wrote the manuscript. Drs. M. Sridhar and J.K. Tsou supervised patient data acquisition, trained sonographers for this study, developed the data processing methods, and trained Y. Qiu, and generated initial strain images for each patient. Dr. K.K. Lindfors identified and recruited patients and consulted on diagnoses. Dr. M.F. Insana organized the team, oversaw the project, and edited the manuscript.

All authors have reviewed and approved the manuscript.

#### REFERENCES

1. American Cancer Society (2007). *Cancer Facts & Figures 2007*. Atlanta, GA: American Cancer Society, 2007.
2. Insana MF, Wickline SA. Multimodality biomolecular imaging. *Proc IEEE* 2008; 96:378–381.
3. Moirand F, Man YG, Arnould L, Bratthauer GL, Ratscheck M, Tavassoli FA. Concurrent and independent genetic alterations in the stromal and epithelial cells of mammary carcinoma: implications for tumorigenesis. *Can Res* 2000; 60:2562–2566.
4. Greenleaf JF, Fatemi M, Insana M. Selected methods for imaging elastic properties of biological tissues. In Martin Yarmush, ed. *Annual Review of Biomedical Engineering*, Palo Alto, CA: Annual Reviews, 2003; 5:57–78.
5. Lerner R, Parker K. Sonoelasticity imaging. *Acoustic Imag* 1988; 17: 317–327.
6. Sinkus R, Tanter M, Xydeas T, Catheline S, Bercoff J, Fink M. Viscoelastic shear properties of in vivo breast lesions measured by MR elastography. *Magn Reson Imaging* 2005; 23:159–165.
7. Fatemi M, Greenleaf J. Ultrasound stimulated vibro-acoustic spectrography. *Science* 1998; 280:82–85.
8. Sharma A, Soo M, Trahey G, Nightingale K. Acoustic radiation force impulse imaging of in vivo breast masses. *Proc IEEE Ultrason Symp* 2004; 728–731.
9. Sridhar M, Insana MF. Ultrasonic measurements of breast viscoelasticity. *Med Phys* 2007; 34:4757–4767.
10. Thomas A, Kümmel S, Fritzsche F, Warm M, Ebert B, Hamm B, Fischer T. Real-time sonoelastography performed in addition to B-mode ultrasound and mammography: improved differentiation of breast lesions. *Acad Radiol* 2006; 13:1496–1504.
11. Thomas A, Warm M, Hoopmann M, Diekmann F, Fischer T. Tissue Doppler and strain imaging for evaluating tissue elasticity of breast lesions. *Acad Radiol* 2007; 14:522–529.
12. Zhi H, Ou B, Luo BM, Feng X, Wen YL, Yang HY. Comparison of ultrasound elastography, mammography, and sonography in the diagnosis of solid breast lesions. *J Ultrasound Med* 2007; 26:807–815.
13. Itoh A, Ueno E, Tohno E, Kamma H, Takahashi H, Shiina T, Yamakawa M, Matsumura T. Breast disease: clinical application of US elastography for diagnosis. *Radiology* 2006; 239:341–350.
14. Rosen PP. *Rosen's breast pathology*. Philadelphia, PA: Lippincott Williams & Wilkins, 2001.
15. Garra BS, Cespedes EI, Ophir J, Spratt SR, Zurbier RA, Magnant CM, Pennanen MF. Elastography of breast lesions: initial clinical results. *Radiology* 1997; 202:79–86.
16. Insana MF, Pellot-Barakat C, Sridhar M, Lindfors K. Viscoelastic imaging of breast tumor microenvironment with ultrasound. *J Mammary Gland Biol & Neoplasia* 2004; 9:393–404.
17. Du H, Liu J, Barakat C, Insana MF. Optimizing multicompression approaches to breast elasticity imaging. *IEEE Trans Ultrason Ferroelec Freq Control* 2006; 53:90–99.
18. Pellot-Barakat C, Frouin F, Insana MF. Ultrasound elastography based on multiscale estimations of regularized displacement fields. *IEEE Trans Med Imaging* 2004; 23:153–163.
19. Sridhar M, Liu J, Insana MF. Viscoelasticity imaging using ultrasound: parameters and error analysis. *Phys Med Biol* 2007; 52:2425–2443.
20. Losa G, Alini M. Sulphated proteoglycans in the extracellular matrix of human breast tissues with infiltrating carcinoma. *Int J Cancer* 1993; 54:552–557.